Icarus 346 (2020) 113804

Contents lists available at ScienceDirect

Icarus

journal homepage: www.elsevier.com/locate/icarus

Refined model age for Orientale Basin derived from zonal crater dating of its ejecta

Zongyu Yue [a,e], Meiping Yang [a,b], Mengna Jia [a,b], Gregory Michael [c], Kaichang Di [a,e,f], Sheng Gou [a,f,*], Jianzhong Liu [d,e]

[a] State Key Laboratory of Remote Sensing Science, Aerospace Information Research Institute, Chinese Academy of Sciences, Beijing 100101, China
[b] University of Chinese Academy of Sciences, Beijing 100049, China
[c] Institute of Geological Sciences, Freie Unversitaet Berlin, Malteser Strasse 74-100, Haus D, Berlin 12249, Germany
[d] Institute of Geochemistry, Chinese Academy of Sciences, Guiyang 550002, China
[e] CAS Center for Excellence in Comparative Planetology, Hefei 230026, China
[f] State Key Laboratory of Lunar and Planetary Sciences, Macau University of Science and Technology, Macau, China

ARTICLE INFO

Keywords:
Orientale Basin
Impact ejecta
Crater counting
Oblique impact

ABSTRACT

The Orientale basin is the most well-preserved multi-ring impact basin on the Moon and it has been used to define the end of the Early Imbrian Epoch. Thus a precise determination of the absolute model age (AMA) of Orientale Basin is important for lunar geology study. The method of crater size–frequency distribution (CSFD) has been used to date Orientale Baisn in previous studies, and the resultant AMA ranges from 3.68 Ga to 3.8 Ga. The inconsistence may be attributed to the choice of counting area and identified superposed craters. In this research we have mapped 27,093 craters larger than 0.7 km in diameter on the entire ejecta of the Orientale Basin, and derived that the AMAs of the Orientale Basin and the pre-existing luanr suface are $3.80^{+0.0074}_{-0.0079}$ Ga and $\sim 4.14^{+0.019}_{-0.022}$ Ga, respectively. And the knee point of the CSFD of the entire counting area is ~10 km, corresponding to ~ 2 km of the average thickness of the Orientale Basin ejecta. To further analyze the variation of the ejecta thickness of Orientale Basin, the counting area was divided into eight 45-degree subsections. The analysis of the knee points of the CSFD in the subdivided counting areas demonstrates that Orientale Basin was formed by an oblique impact from the south-west, and the impact incidence was between 45° and 20°.

1. Introduction

The Orientale Basin is the most well-preserved multi-ring impact basin and its center is located on the western limb of the Moon (centered at 20°S, 95°W) (e.g., Head, 1974; Hawke et al., 1991; Bussey and Spudis, 2000; Cheek et al., 2013). This basin has attracted much interest from the geology community because it is well-preserved and lacks extensive mare flooding (Spudis et al., 1984; 2014). Orientale Basin has traditionally been considered as an archetype of multi-ring impact structures (Spudis et al., 1984; Hawke et al., 1991; Bussey and Spudis, 2000; Johnson et al., 2016). The formation of Orientale Basin also has important significance for the evolution of the Moon, for example, it has been used to define the ending of the Early Imbrian Epoch (Wilhelms et al., 1987). Thus a precise determination of the absolute model age (AMA) of Orientale Basin is of great importance for lunar geology.

The AMA of the Orientale Basin was mostly studied with the crater size–frequency distribution (CSFD) technique, although other strategies were also tried (e.g., Schaeffer and Husain, 1974; Baldwin, 1987a). The method rests upon the assumption that a given surface unit once existed in a pristine state with no superposed craters, and that time is taken as the unit's formation time (Michael et al., 2012). Then the surface accumulates craters, and the present AMA is determined by fitting the current CSFD to a known crater production function (PF) (e.g., Hartmann et al., 1981; Neukum, 1983; Neukum et al., 2001). The crater frequency for certain crater sizes is used together with a calibrating chronology function (CF) to obtain an AMA (Stöffler and Ryder, 2001; Michael and Neukum, 2010). The selected area and superposed craters within a given unit has a significant influence on deriving the AMA with the CSFD method (Arvidson et al., 1979; Michael et al., 2016), which can be demonstrated in previous studies. For example, the AMA of the Orientale Basin was estimated as 3.8 Ga by Wilhelms et al. (1987) with 38 craters mapped by Neukum et al. (1975) and a few craters larger than

* Corresponding author at: P.O. Box 9718, No. 20A, Datun Road, Chaoyang District, Beijing 100101, China.
E-mail address: gousheng@radi.ac.cn (S. Gou).

https://doi.org/10.1016/j.icarus.2020.113804
Received 1 December 2019; Received in revised form 5 March 2020; Accepted 3 April 2020
Available online 13 April 2020

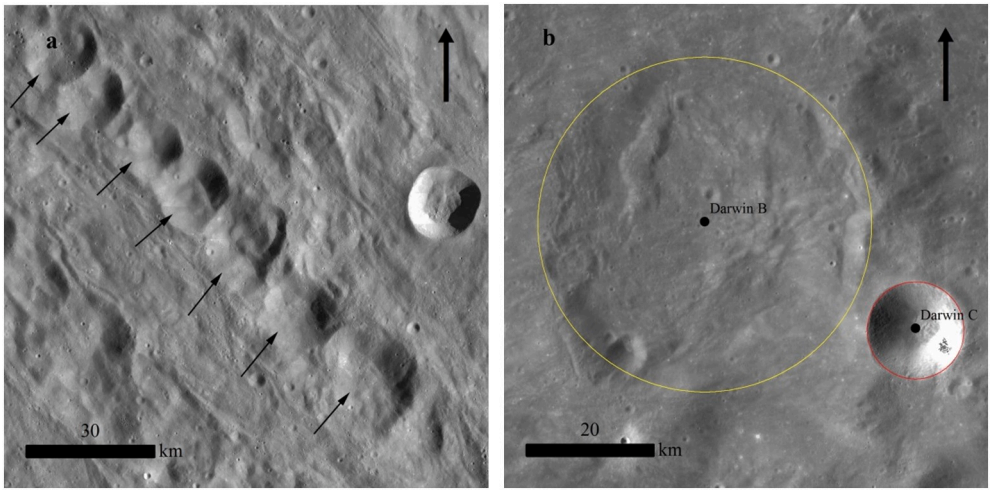

Fig. 1. Exemplified craters in the counting area. (a) Secondary craters from Orientale Basin as indicated by arrows were excluded from the dating process. (b) Both the craters formed before (e.g., Darwin B Crater) and after (e.g., Darwin C Crater) were included in the analysis of the AMA of the Orientale Basin.

20 km in diameter on the Orientale Basin ejecta. Similar work was carried out by Baldwin (1987b) with the result of ~3.79 Ga. Recently Whitten et al. (2011) updated the AMA for Orientale Basin to ~3.68 Ga with the counted craters in diameters between 1 km and 20 km in and around Orientale Basin.

To give a comprehensive analysis of the AMA of the Orientale Basin, the entire ejecta surrounding Orientale Basin was mapped as the counting area (~1.68×10^6 km^2). All of the craters larger than 0.7 km in diameter are counted in this research. Our result indicates the AMA of Orientale Basin is $3.78^{+0.0047}_{-0.0049}$ Ga using the production function of Neukum (1983), and the result is helpful to constrain a more precise chronology in lunar study.

2. Materials and method

Craters superposed on Orientale Basin ejecta were identified in orbital images from Lunar Reconnaissance Orbiter Camera (LROC) Wide Angle Camera (WAC). The WAC is a push-frame camera with resolutions of 75 and 384 m (at an altitude of 50 km) in the visible and ultraviolet bands, respectively (Robinson et al., 2010). LROC WAC covers a swath ~104 km wide from the nominal 50-km orbit (Robinson et al., 2010), which allowed the instrument team to create a number of global mosaics with favorable quality. In this research, the WAC global mosaic created in June 2013 (https://astrogeology.usgs.gov/search/map/Moon/LRO/LROC_WAC/Lunar_LRO_LROC-WAC_Mosaic_global_100m_June2013) (Sato et al., 2014; Wagner et al., 2015) was used as the base map for crater identification and measurement. The area of Orientale Basin ejecta is from the renovated 1:5,000,000 lunar digital geologic maps (Fortezzo and Hare, 2013).

The craters were mapped with an ArcGIS add-in "CraterTools", which can measure the crater boundary and diameter with regard to the map projection (Kneissl et al., 2011). CraterTools can work well with three points identified on the crater rims. The three points should be evenly distributed in order to eliminate any possible errors (Yue et al., 2019). The secondary craters formed on the Orientale Basin ejecta, which were distributed in chains (Fig. 1a), were excluded in the dating process (e.g., McEwen and Bierhaus, 2006; Michael et al., 2012). The craters in the counting area may be superposed on or overlaid with Orientale Basin ejecta (Fig. 1b), and only the former can be used to determine the AMA of the Orientale Basin. However, it is unnecessary to make such distinction between the two types of craters because the ejecta formation process is also considered as a partial resurfacing event (Michael and Neukum, 2010). Another tool used in this study to determine the AMA is the CraterStats2 (Michael and Neukum, 2010), in

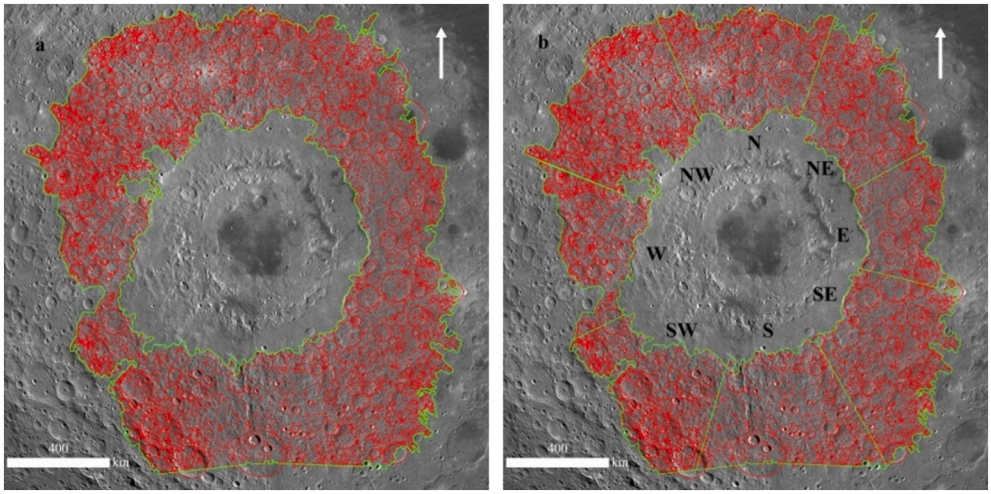

Fig. 2. Counting area (outlined by green polygon) and mapped craters (indicated by red circle) in the research. (a) 27,093 craters larger than 0.7 km in diameter were mapped in the Orientale Basin ejecta. (b) The counting area is further divided into eight subsections for analysis. All the mapped craters and counting areas are available upon request. (For interpretation of the references to colour in this figure legend, the reader is referred to the web version of this article.)

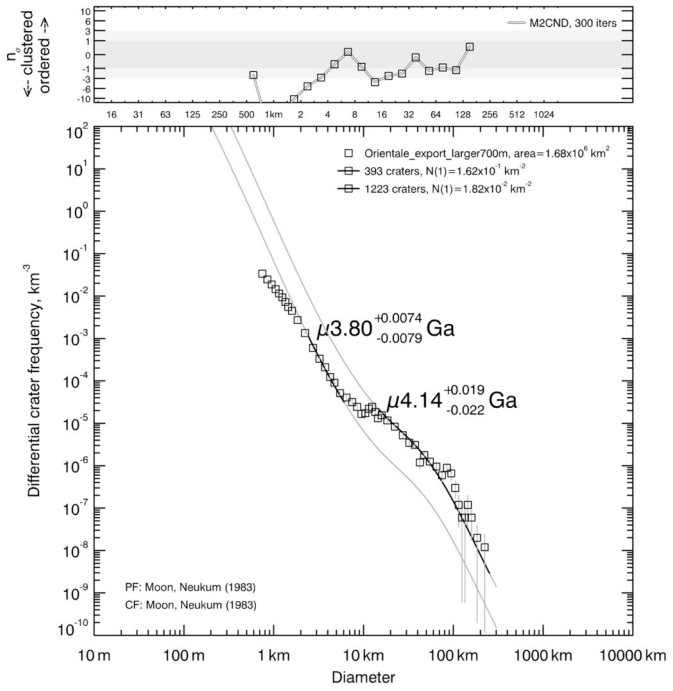

Fig. 3. Dating results of Orientale Basin and the lunar surface time. μ is a function representing the uncertainty of calibration of the chronology model (Michael et al., 2016).

which the Neukum (1983) production and chronology functions are adopted. The dating result is expressed as a likelihood function with an intrinsic uncertainty, which is derived from Poisson statistics and Bayesian inference (Michael et al., 2016).

3. Results

Fig. 2 shows the counting area and mapped craters in this research. In total, 27,093 craters larger than 0.7 km in diameter were mapped in the Orientale Basin ejecta. The mapped crater dataset and their information are listed in supplementary material, and an additional 13,247 smaller craters are also available through the corresponding author. The craters larger than 0.7 km in diameter are used to estimate the AMA of the Orientale Basin.

Fig. 3 shows the dating results with the mapped craters. The larger craters ($D > 11.5$ km) of the distribution lie on the 4.14 Ga isochron, while the distribution flattens toward smaller diameters and then increases in slope. After that the crater distribution follows the 3.80 Ga isochron in the diameter range ~2.8–5.5 km, and the corresponding craters are randomly distributed (Fig. 3). According to Fig. 3, the 4.14 Ga is simply interpreted as the AMA of the pre-existing surface before Orientale formed, and we acknowledge that the underlying surface should have a variety of AMAs, including older ones, as shown in the large crater end of the crater size frequency distribution curve (Fig. 3). The crater population then increased in accordance with the production function until the Orientale Basin-forming impact event occurred. The ejecta from the impact event reduced the population of craters below ~11.5 km in diameter, and likely removed all the craters below ~5.5 km in diameter. After the impact event, the population of craters less than ~5.5 km in diameter began to build up again and followed the 3.80 Ga isochron, which represents the AMA of the Orientale Basin according to the interpretation to the CSFD including resurfacing event (Michael and Neukum, 2010). Because the ejecta coverage is very uneven, the kink of the crater size frequency distribution between two isochron curves is not sharp although the emplacement is near instantaneous. It should be noted that the fall-off at the smallest diameters (~1.6 km and less) is a consequence of the resolution limit of the LROC mosaic image used to make the crater counts, and is a commonly observed effect.

Fig. 4 shows the dating result of each sub-sector in Fig. 2b. The dating results are from 3.74 Ga to 3.85 Ga for Orientale Basin, and from 4.09 Ga to 4.18 Ga for the terrain where Orientale Basin formed. The difference is most likely from the unevenness of ejecta coverage, which makes it difficult to completely separate superposed from underlying craters. The thickness of coverage may vary from sector to sector. It is as expected that the dating results of Orientale impact event and pre-Orientale surface are generally consistent to those in Fig. 3, and the inconsistency is from the counting areas and mapped craters as discussed before.

4. Implications to the Orientale Basin impact

Fig. 3 also provides information on the depth of the Orientale Basin ejecta. It can be assumed an old terrain appears at ~ 4.14 Ga, and then the impact for the formation of Orientale Basin happened at ~3.80 Ga. Besides the many craters which are removed directly by the impact, pre-existing craters surrounding Orientale Basin are covered by the thick ejecta. For the largest craters with great depth, they can be still identified as exemplified by Darwin B Crater in Fig. 1b. As a result, a transition interval between two isochrons appears in the CSFD. The transition interval corresponds to the diameters of the buried pre-existing craters, with its width depending mainly on the inhomogeneous depth of the ejecta (other factors, such as the pre-existing topography and random spatial distribution of the craters may also have contributed). For the Orientale Basin, the transition interval of the crater diameters are 5.7–12.6 km. If 12.6 km is considered as the diameter of the largest buried crater in the ejecta of Orientale Basin, the ejecta depth surrounding the Cordillera Mountain ring would be ~2.52 km. This value is 13% smaller than that ~2.9 km estimated by Fassett et al. (2011) with Lunar Orbiter Laser Altimeter (LOLA) data. This discrepancy may be caused by the randomness of crater spatial distribution and inherent uncertainty of the CSFD method, although it can give an estimation of the ejecta depth surrounding one crater.

Analysis of the thickness of Orientale Basin ejecta can also provide some information on the ejecta structure as a whole. However, it is necessary to derive a representative thickness for the measured area because of the existence of transition interval of the crater diameters. As the ejecta thickness t may be represented by a power function of distance from the crater center (McGetchin et al., 1973):

$$t = 0.14R^{0.74}\left(\frac{r}{R}\right)^{-3.0} \quad (1)$$

where r is the range measured radially from the center of the crater and R is the crater radius (all measured in meters). The above equation can be modified as:

$$r = R\left(0.14R^{0.74}\right)^{1/3}t^{-1/3} \quad (2)$$

The thickness of the ejecta in the mid-point between the radial distances of r_1 and r_2 is:

$$t_m = 8\left(t_1^{-1/3} + t_2^{-1/3}\right)^{-3.0} \quad (3)$$

According to the scaling law (Melosh, 1989), the depth of the crater is about 1/5 of the diameter. Therefore, the above equation can be further modified with the transited crater diameters:

$$t_m = 0.2\left(D_{\min}^{-1/3} + D_{\max}^{-1/3}\right)^{-3.0} \quad (4)$$

where $D_{\min}$ and $D_{\max}$ correspond to the minimum and maximum diameter of the transition interval, respectively. The parameter t_m, which is named average thickness, will be used to represent the thickness of the ejecta in each sub-sector. In addition, if the different relationships for the ejecta thickness and the distance from the crater

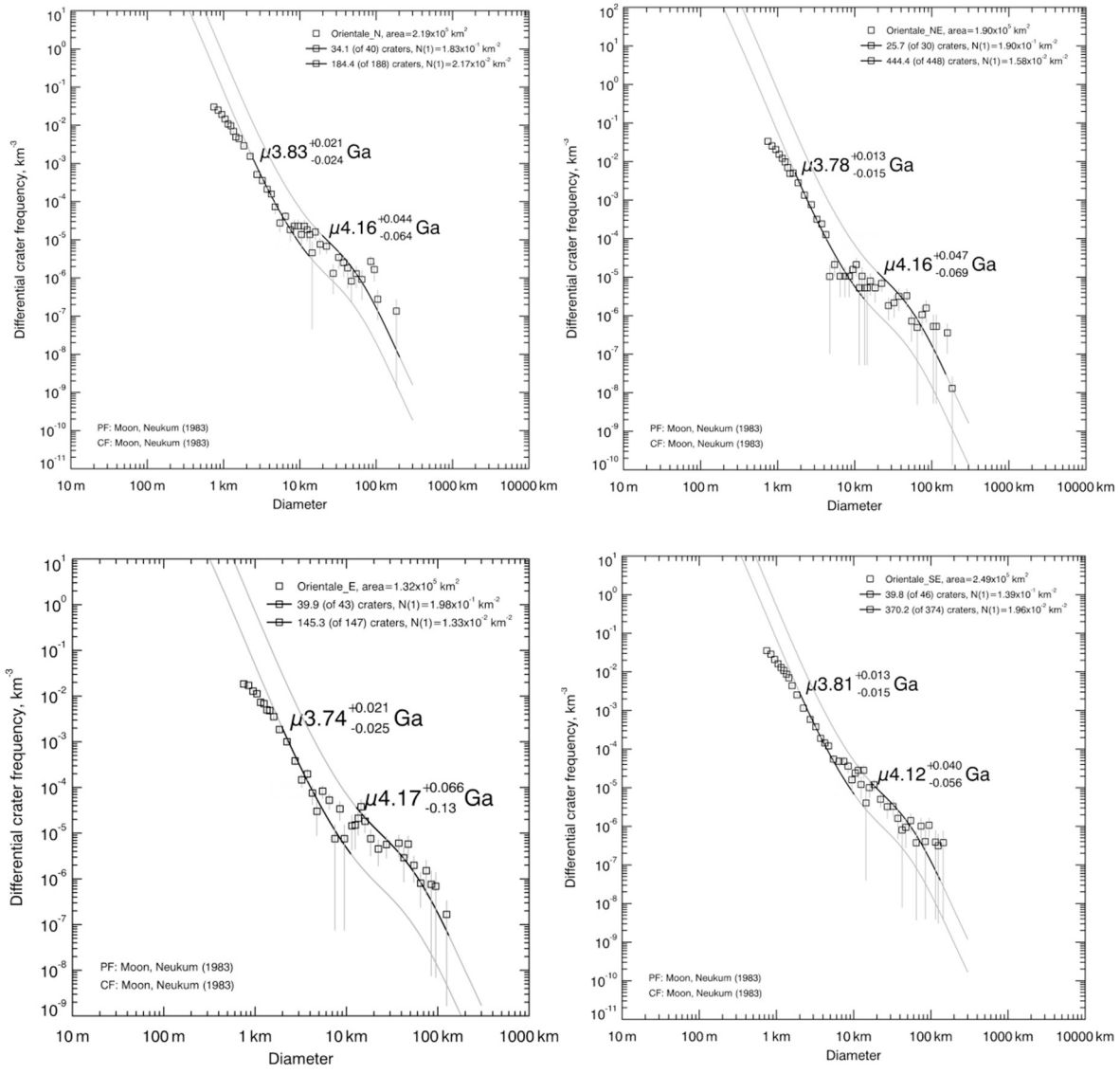

Fig. 4. Dating results of the eight sub-sectors as shown in Fig. 3b. μ is a function representing the uncertainty of calibration of the chronology model (Michael et al., 2016).

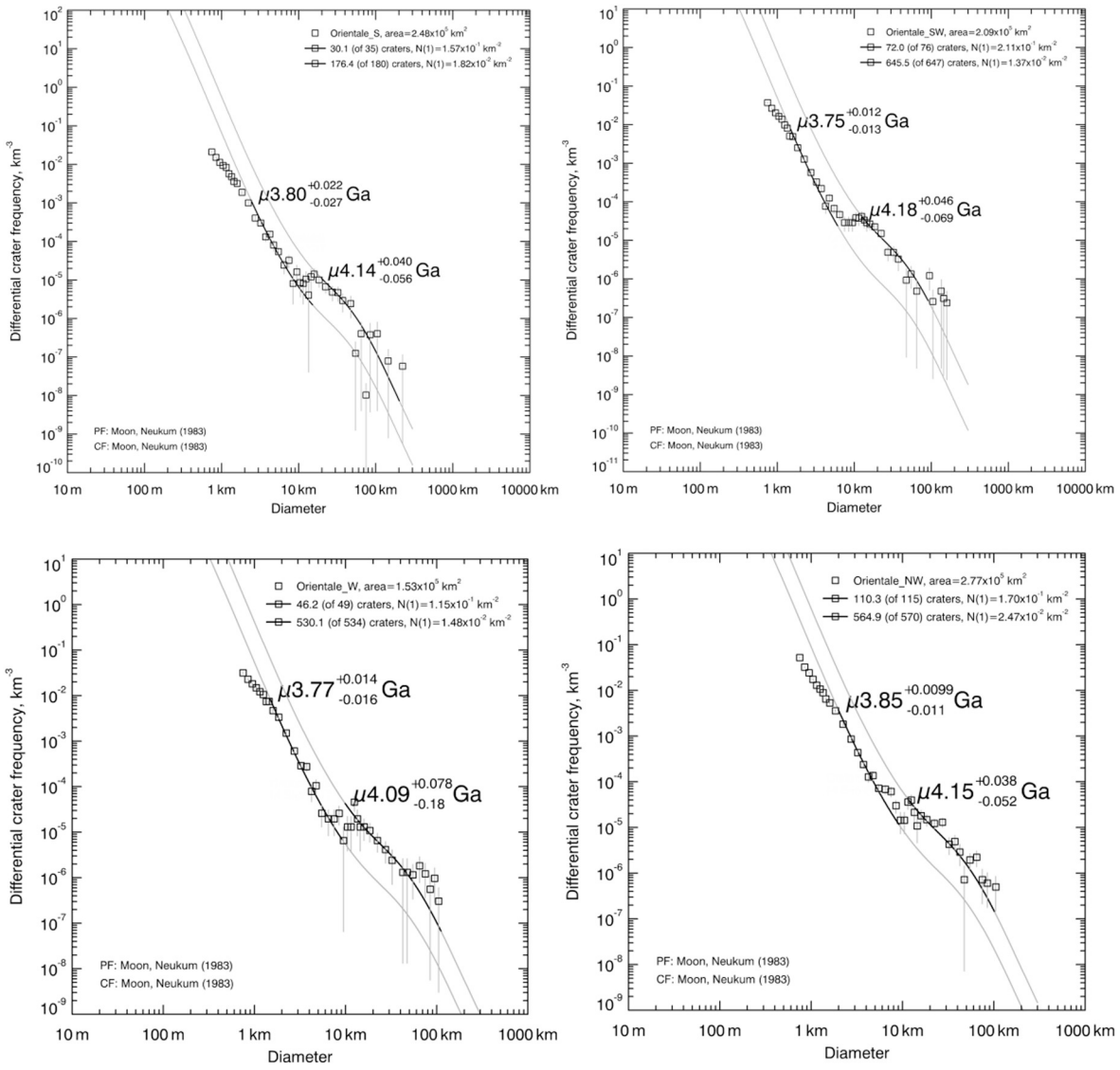

Fig. 4. (*continued*).

center are adopted (e.g., Petro and Pieters, 2006), similar equations would be derived with different powers in Eq. (4). The inherent significance of the above equation is the thickness of the ejecta at half of the radial distance, if the craters are always randomly distributed.

As the transition interval of the crater diameters are 5.7–12.6 km for the Orientale Basin, the representative depth of the ejecta is ~206 m. Similar analysis can also be carried for the sub-sectors with the results from Fig. 4. As shown in Fig. 4, the transitional diameter interval of each sub-sector of Orientale Basin ejecta is different. Fig. 5 shows the derived ejecta thickness within eight different sub-sectors, and Table 1 lists the corresponding values.

It can be seen that the thicknesses of the ejecta in sub-sectors in South (435 m), NorthEast (403 m), and North (403 m) are much larger than that in other sub-sectors, and the ejecta in sub-sectors of SouthWest (206 m), West (237 m), and East (313 m) are much thinner. The variation on thickness may imply that a forbidden zone has been developed in the southeast during the Orientale Basin-forming impact. For simple and complex craters, previous studies on ejecta formed by oblique impact (e.g., Gault and Wedekind, 1978; Melosh, 1989; Schultz, 1999) suggested that a wedge-shaped forbidden zone would develop uprange when the incidence angle is between 45° and 20° in the situation of the simple crater. In the case of large impact basins, it is reasonable to conceive that some ejecta will also appear in the uprange of the crater with similar impact conditions. Therefore, the result may be interpreted that the Orientale Basin was most likely formed by an oblique impact and the incidence angle possibly was between 45° and 20°.

On the impact direction, Schultz and Papamarcos (2010) deduced the impact for Orientale Basin is from the northeast toward the southwest according to the distribution of grooves and elongated secondaries. Morse et al. (2018) believed that Orientale was formed by an oblique impact from the northeast based on the lack of secondary impact crater chains to the northeast. Guo et al. (2018) also deduced that the impact for Orientale Basin is from the northeast based on the distribution density of the secondaries. It can be seen that these studies are mostly obtained from the secondaries of the Orientale Basin. However, in the northeast of Orientale Basin, the maria basalt in Oceanus Procellarum is widely distributed and most of their AMAs are younger than Orientale Basin (~99.74%; Hiesinger et al., 2003). As a result, a significant fraction of the secondaries in the northeast would be flooded by mare basalts. The previous studies may have missed some secondaries and derived inconvincible conclusion. The previous deduced impact direction is also inconsistent with the representative ejecta thickness of each sub-sector derived in this study, i.e., the ejecta thickness is much higher in the South, NorthEast, and North than that in the opposite sectors.

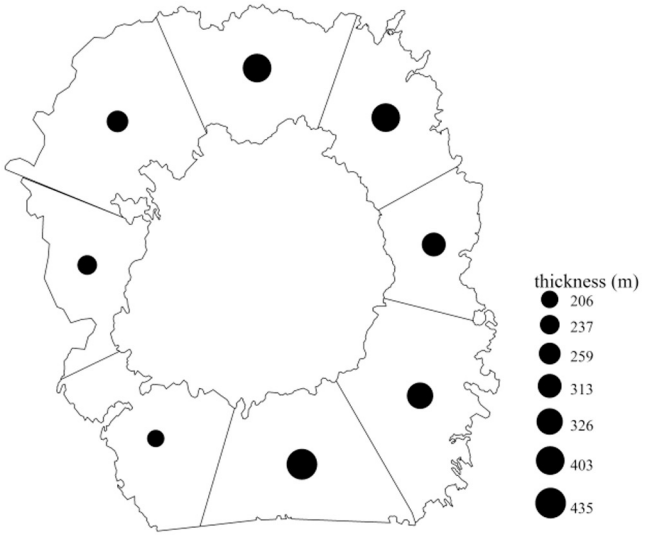

Fig. 5. Variations of the average thickness of Orientale Basin ejecta in sub-sectors. The thicknesses are derived from the minimum transition diameter of the craters in Fig. 4 for each sub-sector. The corresponding values are listed in supporting online material Table 1.

Table 1
Depth of the ejecta in eight sub-sections.

Sub-sector	Diameter interval (km)	Representative ejecta depth (m)
E	11.2–14.1	313
N	13.2–20.0	403
NE	13.5–19.5	403
NW	9.2–11.7	259
S	15.2–20.0	435
SE	10.0–17.4	326
SW	5.9–12.0	206
W	8.96–10.1	237

Therefore, we suggest that the interpretation on the impact direction should be cautious and further studies are necessary on this topic.

5. Conclusion

In this research we mapped the craters on the entire Orientale Basin ejecta, and the dating result with the crater counting method indicates that Orientale Basin formed $\mu 3.80^{+0.0074}_{-0.0079}$ Ga ago on the $\mu 4.14-^{+0.0019}_{-0.0022}$ Ga old pre-existing lunar surface. The analysis of the knee points on sub-divided counting areas provides information on the ejecta thickness of Orientale Basin, i.e., the ejecta is much thicker in South, NorthEast, and North and much thinner in SouthEast, NorthEast, and East. The ejecta thickness estimates indicate that Orientale was most likely formed by an oblique impact.

Acknowledgements

The authors gratefully acknowledge LROC team for providing LRO WAC mosaic image. The authors also thank Thomas Kneissl for the software CraterTools. This work was supported by the B-type Strategic Priority Program of the Chinese Academy of Sciences (grant No. XDB41000000) and National Natural Science Foundation of China (grant Nos. 41972321, 41590851, and 41702354), Macao Young Scholars Program (grant No. AM201902), and the Science and Technology Development Fund of Macao (grant no. 131/2017/A3). Constructive reviews by two anonymous reviewers improved the quality of this manuscript substantially, and are greatly appreciated.

Appendix A. Supplementary data

Supplementary data to this article can be found online at https://doi.org/10.1016/j.icarus.2020.113804.

References

Arvidson, R.E., Boyce, J., Chapman, C., et al., 1979. Standard techniques for presentation and analysis of crater size-frequency data. Icarus 37, 467–474.
Baldwin, R.B., 1987a. On the relative and absolute ages of seven lunar front face basins: I. From viscosity arguments. Icarus 71, 1–18.
Baldwin, R.B., 1987b. On the relative and absolute ages of seven lunar front face basins: II. From crater counts. Icarus 71, 19–29.
Bussey, D.B.J., Spudis, P.D., 2000. Compositional studies of the Orientale, Humorum, Nectaris, and Crisium lunar basins. J. Geophys. Res. 105, 4235–4243.
Cheek, L.C., Donaldson Hanna, K.L., Pieters, C.M., Head, J.W., Whitten, J.L., 2013. The distribution and purity of anorthosite across the Orientale basin: new perspectives from Moon Mineralogy Mapper data. J. Geophys. Res. 118 https://doi.org/10.1002/jgre.20126.
Fassett, C.I., Head, J.W., Smith, D.E., Zuber, M.T., Neumann, G.A., 2011. Thickness of proximal ejecta from the Orientale Basin from Lunar Orbiter Laser Altimeter (LOLA) data: implications for multi-ring basin formation. Geophys. Res. Lett. 38, L17201.
Fortezzo, C.M., Hare, T.M., 2013. Completed digital renovation of the 1:5,000,000 lunar geologic map series. In: 44th Lunar and Planetary Science Conference, Abstract #2114.
Gault, D.E., Wedekind, J.A., 1978. Experimental studies of oblique impact. In: Proc. Lunar Planet. Sci. Conf. 9th, pp. 3843–3875.
Guo, D., Liu, J., Head III, J.W., Kreslavsky, M.A., 2018. Lunar Orientale impact basin secondary craters: spatial distribution, size-frequency distribution, and estimation of fragment size. Journal of Geophysical Research: Planets 123.
Hartmann, W.K., Strom, R.G., Weidenschilling, S.J., Blasius, K.R., Voronow, A., Dence, M.R., Grieve, R.A.F., Diaz, J., Chapman, C.R., Shoemaker, E.M., Jones, K.L., 1981. Chronology of Planetary Volcanism by Comparative Studies of Planetary Craters. Basaltic Volcanism on the Terrestrial Planets. Pergamon Press, Elmsford, NY, pp. 1050–1127.
Hawke, B.R., Lucey, P.G., Taylor, G.J., Bell, J.F., Peterson, C.A., Blewett, D.T., Horton, K., Smith, G.A., 1991. Remote sensing studies of the Orientale region of the Moon: a pre-Galileo view. Geophys. Res. Lett. 18, 2141–2144.
Head, J.W., 1974. Orientale multi-ringed basin interior and implications for the petrogenesis of lunar highland samples. Moon 11, 327–356.
Hiesinger, H., Head III, J.W., Wolf, U., Jaumann, R., Neukum, G., 2003. Ages and stratigraphy of mare basalts in Oceanus Procellarum, Mare Nubium, Mare Cognitum, and Mare Insularum. J. Geophys. Res. 108 (E7), 5065.
Johnson, B.C., Blair, D.M., Collins, G.S., et al., 2016. Formation of the Orientale lunar multiring basin. Science 354, 441–444.
Kneissl, T., van Gasselt, S., Neukum, G., 2011. Map–projection–independent crater size-frequency determination in GIS environments–new software tool for ArcGIS. Planetary and Space Science 59, 1243–1254.
McEwen, A.S., Bierhaus, E.B., 2006. The importance of secondary cratering to age constraints on planetary surfaces. Annual Review of Earth & Planetary Sciences 34, 540–567.
McGetchin, T.R., Settle, M., Head, J.W., 1973. Radial thickness variation in impact crater ejecta, implication for lunar basin deposits. Earth Planet. Sci. Lett. 20, 226–236.
Melosh, H.J., 1989. Impact Cratering: A Geologic Process. Oxford University Press, New York.
Michael, G.G., Neukum, G., 2010. Planetary surface dating from crater size–frequency distribution measurements: partial resurfacing events and statistical age uncertainty. Earth Planet. Sci. Lett. 294, 223–229.
Michael, G.G., Platz, T., Kneissl, T., Schmedemann, N., 2012. Planetary surface dating from crater size–frequency distribution measurements: spatial randomness and clustering. Icarus 218, 169–177.
Michael, G.G., Kneissl, T., Neesemann, A., 2016. Planetary surface dating from crater size-frequency distribution measurements: Poisson timing analysis. Icarus 277, 279–285.
Morse, Z.R., Osinski, G.R., Tornabene, L.L., 2018. New morphological mapping and interpretation of ejecta deposits from Orientale Basin on the Moon. Icarus 299, 253–271.
Neukum, G., 1983. Meteoriten Bombardement Und Datierung Planetarer Oberflachen Habilitation Thesis for Faculty Membership. Univ. of Munich. 186 pp. (English Translation, 1984: Meteorite Bombardment and Dating of Planetary Surfaces). Habilitation Thesis. University München, Munich, Germany.
Neukum, G., König, B., Arkani-Hamed, J., 1975. A study of lunar impact crater size-distributions. The Moon 12, 201–229.
Neukum, G., Ivanov, B.A., Hartmann, W.K., 2001. Cratering records in the inner solar system in relation to the lunar reference system. Space Sci. Rev. 96, 55–86.
Petro, N., Pieters, C.M., 2006. Modeling the provenance of the Apollo 16 regolith. J. Geophys. Res. 111, E09005.
Robinson, M.S., Brylow, S.M., Tschimmel, M., et al., 2010. Lunar Reconnaissance Orbiter Camera (LROC) instrument overview. Space Sci. Rev. 150, 81–124.
Sato, H., Robinson, M.S., Hapke, B., Denevi, B.W., Boyd, A.K., 2014. Resolved Hapke parameter maps of the Moon. Journal of Geophysical Research: Planets 119, 1775–1805.
Schaeffer, O.A., Husain, L., 1974. Chronology of lunar basin formation. Geochimica et Cosmochimica Acta, Supl 5, 1541–1555.

Schultz, P., Papamarcos, S., 2010. Evolving flowfields from imbrium and orientale impacts. In: Lunar and Planetary Science Conference, 41, 2480, Houston, TX.
Schultz, P.H., 1999. Ejecta distribution from oblique impacts into particulate targets. In: Lunar Planet. Sci. Conf. 30, Abstr. #1919.
Spudis, P.D., Hawke, B.R., Lucey, P.G., 1984. Composition of Orientale basin deposits and implications for the lunar basin-forming process. J. Geophys. Res. 89, C197–C210 suppl.
Spudis, P.D., Martin, D.J.P., Kramer, G., 2014. Geology and composition of the Orientale basin impact melt sheet. J. Geophys. Res. Planets 119, 19–29. https://doi.org/10.1002/2013JE004521.
Stöffler, D., Ryder, G., 2001. Stratigraphy and isotope ages of lunar geologic units: chronological standard for the inner solar system. Space Sci. Rev. 96, 9–54.
Wagner, R.V., Speyerer, E.J., Robinson, M.S., LROC Team, 2015. New mosaicked data products from the LROC team. In: 46th Lunar and Planetary Science Conference (Abstract #1473).
Whitten, J., Head, J.W., Staid, M., Pieters, C.M., Mustard, J., Clark, R., Nettles, J., Klima, R.L., Taylor, L., 2011. Lunar mare deposits associated with the Orientale impact basin: new insights into mineralogy, history, mode of emplacement, and relation to Orientale Basin evolution from Moon Mineralogy Mapper (M3) data from Chandrayaan-1. J. Geophys. Res. 116, E00G9.
Wilhelms, D.E., McCauley, J.F., Trask, N.J., 1987. The geologic history of the Moon. USGS Professional Paper 1348, 302.
Yue, Z., Di, K., Liu, Z., Michael, G., Jia, M., Xin, X., Liu, B., Peng, M., Liu, J., 2019. Lunar regolith thickness deduced from concentric craters in the CE-5 landing area. Icarus 331, 116–126.